# Magnetophotoselection Study of the Carotenoid Triplet State in *Rhodobacter sphaeroides* Reaction Centers

**Igor V. Borovykh,[†] Irina B. Klenina,[‡] Ivan I. Proskuryakov,[‡] Peter Gast,[†] and Arnold J. Hoff*,[†]**

*Department of Biophysics, Huygens Laboratory, P.O. Box 9504, 2300 RA Leiden, The Netherlands and Institute of Basic Biological Problems RAS, Pushchino, 142290, Russia*

*Received: July 9, 2001; In Final Form: December 12, 2001*

The triplet state of the carotenoid spheroidene, a pigment cofactor of reaction centers (RCs) from the photosynthetic bacterium *Rhodobacter sphaeroides* 2.4.1., was studied with time-resolved direct-detection EPR under polarized light excitation (magnetophotoselection). Four types of magnetophotoselection experiments, differing by excitation wavelength and temperature, enabled determination of the orientations of the optical transition moments of the reaction center spheroidene and the primary donor relative to the principal triplet axes of these molecules. Making use of the projections of the primary donor principal triplet axes onto the X-ray structural coordinate system determined earlier, we were able to calculate for the first time the orientation of the spheroidene optical transition moment and its principal triplet axes relative to the RC molecular frame. The same type of experiment on carotenoidless reaction centers from *Rb. sphaeroides* R26 reconstituted with spheroidene demonstrated a significant difference between the native and reconstituted molecules with regard to the orientation of the optical transition moment of the carotenoid relative to its triplet principal axes frame.

## Introduction

Carotenoids (Car) are universally found in living organisms. In photosynthetic bacteria, they, together with bacteriochlorophylls (BChls), represent the major pigments of photosynthetic membranes.[1] It is well established that in photosynthesis, carotenoids fulfill light-harvesting and protective roles[2,3] and are located both in the antennae systems and in the reaction centers (RCs). In the reaction centers, they absorb light and transfer excitation energy to BChls, filling the blue-green spectral region where BChl molecules absorb weakly.[1] For several photosynthetic bacteria, they in addition have a protective function, quenching the triplet states of BChls and thus preventing the sensitized formation of harmful singlet oxygen or quenching singlet oxygen itself.[2−4] In this work, reaction center preparations of *Rhodobacter (Rb.) sphaeroides* are studied, which contain the carotenoid spheroidene. Below we review the results obtained for this photosynthetic bacterium.

Carotenoid photophysics, especially of its triplet states ($^3$Car), is not well studied. This is due to very low triplet quantum yields of the molecules in vitro resulting from the high rate of their radiationless decay. In recent work,[5] it was shown that the optically allowed $S_2$ ($^1B_u$*) excited state of spheroidene in solution has a lifetime of only 8 ± 1 ps. Population of the $^3$Car state by direct excitation of carotenoid and intersystem crossing proved successful mostly when intermolecular interactions were present, that is, in Car-containing micelles,[6] biological membranes,[7] or carotenoid crystals.[8] In these instances, $^3$Car population proceeds by a very fast process of singlet excitation fission into two carotenoid triplets.[9] Another way to populate carotenoid triplets in solution is to use triplet sensitizers, such as naphthalene, anthracene, or chlorophyll.[10] The triplet state of an RC-bound carotenoid is populated in a similar way. When functional electron transfer in RCs is blocked, the triplet state of the so-called primary electron donor (BChl dimer, P) is populated by the recombination of photoinduced radicals (radical pair mechanism) with unique $T_0$ spin polarization.[11,12] The triplet state of the carotenoid is formed by quenching of the primary donor triplet state (T−T energy transfer). Because of conservation of spin angular momentum, the spin polarization of $^3$Car is the same as that of $^3$P, that is, only $T_0$ level is populated. However, the polarization pattern, observed in the $^3$Car EPR spectrum, is inverted because the sign of zero-field splitting (ZFS) constant D (negative) in $^3$Car is opposite to that of $^3$P.[13] The quantum yield of $^3$P varies with temperature, increasing from ca. 0.14 at 300 K to about 1 below 77 K.[14,15] On the contrary, the yield of $^3$Car is low at $T < 30$ K and increases above this point. Such behavior was explained by the presence of an intermediary thermoactivated stage of the T−T energy transfer from $^3$P to Car,[16] which is most probably the population of the triplet state of the monomeric bacteriochlorophyll located between P and Car.[17,18] The current scheme of the $^3$Car population looks as follows:

$$^1P^*\Phi Car \rightarrow {}^1[P^+\Phi^-]Car \rightarrow {}^3[P^+\Phi^-]Car \rightarrow {}^3P\Phi Car \xrightarrow{T > 30\ K} {}^1P\Phi {}^3Car \rightarrow {}^1P\Phi Car$$

where Φ stands for the active bacteriopheophytin molecule of the RC, and the intermediary monomeric BChl triplet is not shown. Thus, by varying the temperature, the triplet states $^3$P and $^3$Car can be populated almost selectively and studied separately. This makes reaction centers a very attractive object for studies of the carotenoid triplet state. A general review of studies on reaction center triplet states is given in references 19−21. The carotenoid triplet state has been studied both with

* To whom correspondence should be addressed.
[†] Huygens Laboratory.
[‡] Institute of Basic Biological Problems RAS.

10.1021/jp0125810 CCC: $22.00 
Published on Web 04/02/2002

optical spectroscopy[22,23] and with EPR.[6,24,25] Much effort was spent to determine the orientation of the principal triplet axes of the carotenoid spheroidene in the RCs of *Rb. sphaeroides* 2.4.1. utilizing the technique of magnetophotoselection (MPS).[26] In these studies, conventional CW EPR and excitation with amplitude modulated light to improve sensitivity were used. As the $^3$Car state is essentially short-lived, kinetic parameters had to be introduced into the spectral simulation procedure, decreasing the precision of the information obtained from MPS.

Earlier, we demonstrated the feasibility of MPS measurements with CW direct-detection EPR (DDEPR).[27] The advantage of this approach is its time resolution, high enough to measure transient signals before they have relaxed appreciably. In the present work, this technique is applied to the study of the spheroidene triplet state in *Rb. sphaeroides* 2.4.1. reaction centers. By combining our results with crystallographic data from literature, we were able to determine the orientation of the optical transition moment and the principal triplet magnetic axes of the carotenoid relative to the molecular frame. The same set of experiments was performed also on reaction centers of the carotenoidless mutant *Rb. sphaeroides* R26, reconstituted with spheroidene.

## Experimental Section

**Biochemical Procedures.** Reaction center preparations of *Rb. sphaeroides* 2.4.1. (wild type) and of the carotenoidless mutant *Rb. sphaeroides* R26 were used. Cells of the *Rb. sphaeroides* 2.4.1. were grown photosynthetically without oxygen. Reaction centers under such conditions are known to accumulate almost exclusively (>95%) spheroidene.[1,16] RCs from *Rb. sphaeroides* R26 were isolated as described by Feher et al.[28] and those from the wild type as described by Frank et al.[29] The extraction of the spheroidene from aerobically grown *Rb. sphaeroides* 2.4.1 and reconstitution into the *Rb. sphaeroides* R26 reaction centers were done as described in reference 30. All RC preparations were frozen under light in the presence of 10 mM sodium ascorbate to prereduce the primary electron acceptor $Q_A$. This procedure created conditions for $^3$P formation. Typical EPR samples contained 60−70% (v/v) glycerol and were prepared in 3 mm i.d. quartz tubes. Final optical density of the samples was 10−30 $cm^{-1}$ in the primary donor absorption band. The samples were degassed by three freeze−pump−thaw cycles and sealed under vacuum. This procedure decreased the probability of crack formation when cooling the samples. For optical measurements, the samples were diluted to an optical density of 2 per cm and placed in 2.5-mm (inner size) cuvettes. Glycerol was added to obtain a clear glass at low temperature.

**Instrumental.** As an excitation light source, a Continuum Surelite I pumped OPO laser was used with flash duration of ca. 4 ns. The incident energy was attenuated to ca. 0.1 mJ·$cm^{-2}$ at the sample inside the EPR cavity to avoid light saturation of the magnetophotoselection effects. Samples were excited into the near-infrared absorption band of the primary donor at 896 nm (bandwidth ca. 5 nm), which corresponds to the $\boldsymbol{Q_Y}$ transition of P at low temperature for RCs from *Rb. sphaeroides* and into the carotenoid absorption band at 472 nm (bandwidth ca. 1 nm) corresponding to the central peak of the vibronic structure of the spheroidene $S_2 \leftarrow S_0$ optical transition. The technique of magnetophotoselection measurements with DDEPR was described earlier.[27,31] In short, a home-built X-band EPR spectrometer was used with boxcar sampling of the laser flash-induced kinetic EPR signals retrieved directly after the microwave mixer. The EPR transients were recorded with the boxcar gate width of 1.3 $\mu$s delayed for 0.2 $\mu$s after the flash (DAF = 0.2 $\mu$s). In a control experiment, the signals were compared with DAF = 0.2 $\mu$s and 1.0 $\mu$s, with a gate width 0.5 $\mu$s. No difference in the shape of the spin-polarized triplet signals was observed demonstrating the absence of significant relaxation effects. In the DDEPR experiment, the signal appears in direct absorption and emission mode. The overall time resolution of our setup was about 50 ns. The temperature in the Oxford Instruments helium gas-flow cryostat was regulated with a home-built temperature controller, which could be set with 1 K accuracy, and the temperature was stabilized to ±0.2 K.

Room- and low-temperature absorption spectroscopy was performed with a single-beam spectrophotometer described earlier.[32] The spectral resolution was 0.5 nm. Measurements at cryogenic temperatures were performed with an Oxford Instruments helium flow cryostat.

**Simulation Procedures.** The spectral simulations were done as described previously.[27] Two spectra, obtained with the excitation light polarization plane parallel and perpendicular to the magnetic field, were simulated with the same set of parameters, providing the projections of the optical transition moment of the excited molecule with respect to the principal magnetic axes of the triplet-bearing molecule. This orientation is not determined from MPS in a unique way, because MPS is insensitive to the signs of the projections. Thus, all possible sign combinations had to be tested. The resulting vectors of the optical transition moments were then recalculated to the crystallographic coordinate system, using the data of the single-crystal $^3$P study (1PSS structure).[33] In this work, the orientation of the $^3$P principal magnetic axes relative to the X-ray coordinate system was determined, so that any vector specified within the $^3$P magnetic system, as is the case for the MPS measurements, could be overlaid on the molecular structure. In the experiments described below, orientations of the primary donor optical transition moment, $\boldsymbol{Q_Y}$, and that of the carotenoid, $\boldsymbol{D}$, were obtained both in the $^3$P and in the $^3$Car principal magnetic axes systems. This enabled calculation of the $^3$Car magnetic axes relative to the molecular frame of the carotenoid. RasMol version 2.7.1. was used in calculations involving structural data files and for creating Figure 4. Details of the calculations will be presented in the next section.

## Results

**Magnetophotoselection Data and Orientation of Optical Transition Moments in the Principal Triplet Axes Systems.** Taking advantage of the marked difference in the P and Car absorption spectra, so that those molecules can be excited almost selectively, and of the possibility to control population of the $^3$P or $^3$Car states by changing the temperature,[16,25] four types of MPS experiments were designed:

*Type 1*. Direct excitation of P and detection of the $^3$P signal ($\lambda_{exc}$ = 896 nm, $T$ = 10 K) enabled determination of the $\boldsymbol{Q_Y}$ orientation relative to the $^3$P principal axes.

*Type 2*. Direct excitation of P and detection of the $^3$Car signal ($\lambda_{exc}$ = 896 nm, $T$ = 100 K) enabled determination of the $\boldsymbol{Q_Y}$ orientation relative to the $^3$Car principal axes.

*Type 3*. Indirect excitation of P, preceded by S−S energy transfer from the excited Car, and detection of the $^3$Car signal ($\lambda_{exc}$ = 472 nm, $T$ = 100 K) enabled determination of the $\boldsymbol{D}$ orientation relative to the $^3$Car principal axes.

*Type 4*. Indirect excitation of P, preceded by S−S energy transfer from the excited Car, and detection of the $^3$P signal ($\lambda_{exc}$ = 472 nm, $T$ = 10 K) enabled determination of the $\boldsymbol{D}$ orientation relative to the $^3$P principal axes.

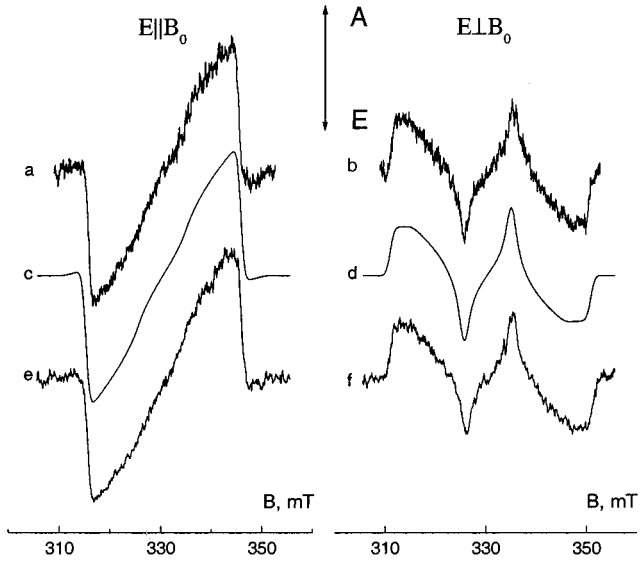


**Figure 1.** Direct-detection EPR spectra of the $^3$P state measured under excitation light polarized parallel (a, e) and perpendicular (b, f) to the magnetic field. $T = 10$ K, $\lambda_{exc.} = 896$ nm (Type 1 experiment), boxcar gate 1.3 $\mu$s, DAF = 0.2 $\mu$s. (a, b): RCs of *Rb. sphaeroides* 2.4.1.; (e, f): additionally purified $Q_A$-depleted RCs of *Rb. sphaeroides* R26; (c, d): spectral simulations performed with the following parameters: $D = 0.0188$ cm$^{-1}$, $E = 0.0033$ cm$^{-1}$, $g_x = g_y = 2.002$, $g_z = 2.000$, $\Delta H_x = \Delta H_y = \Delta H_z = 1.3$ mT. Values of the best-fit angular parameters $\delta$, $\gamma$ are given in Table 1.

Figure 1a, b shows DDEPR spectra of the primary donor triplet state in chemically reduced reaction centers from *Rb. sphaeroides* 2.4.1. The spectra were obtained in a Type 1 experiment with two different polarizations of the excitation light, (a) parallel to the magnetic field and (b) perpendicular to the magnetic field. In the following, these spectra will be referred to as the $\mathbf{E}||\mathbf{B_0}$ and $\mathbf{E}\perp\mathbf{B_0}$ spectra, respectively. The best fits of the experimental data are shown in Figure 1c, d. They were calculated for the orientation of $\boldsymbol{Q_Y}$ relative to the $^3$P principal magnetic axes ($x$, $y$, $z$ axes of $^3$P zero-field splitting tensor) determined by the angles $\delta = 90° \pm 10°$, $\gamma = 90° \pm 10°$ ($\delta$ and $\gamma$ are the spherical coordinates of $\boldsymbol{Q_Y}$;[27] the angles in the first octant are given). These values are slightly different from the values of $\delta = 80 \pm 5°$, $\gamma = 70 \pm 5°$ obtained earlier[27] for the orientation of the optical transition moment of primary donor relative to $^3$P magnetic axes in the RCs from carotenoidless mutant of *Rb. sphaeroides* R26. However small the difference is, it is of a special importance because the single-crystal EPR study of $^3$P, which relates the principal magnetic axes of the primary donor triplet to the X-ray structure of the RC, is available only for the R26 mutant strain of *Rb. sphaeroides*.[33] When using this information for transforming vectors determined in the $^3$P principal coordinate system of *Rb. sphaeroides* 2.4.1. into the crystallographic axes system, one has to be certain that the properties of P are the same as those of the primary donor of the R26 mutant. The X-ray structures of P in both RCs are almost identical.[34,35] The values of the angles cited above, however, point to some difference in the relative orientations of the optical transition moments and triplet magnetic axes systems, which would preclude us from using the single-crystal EPR data for the purposes of the present work. We therefore have probed further into the properties of the $^3$P state in the *Rb. sphaeroides* R26 RC preparation used earlier.[27] Excitation of $Q_A$-depleted reaction centers at 850 nm resulted in a $^3$P MPS spectra (Figure 2a, b, dots) different from that obtained earlier for excitation at 900 nm with a similar preparation.[27] The most prominent features are the apparent wide

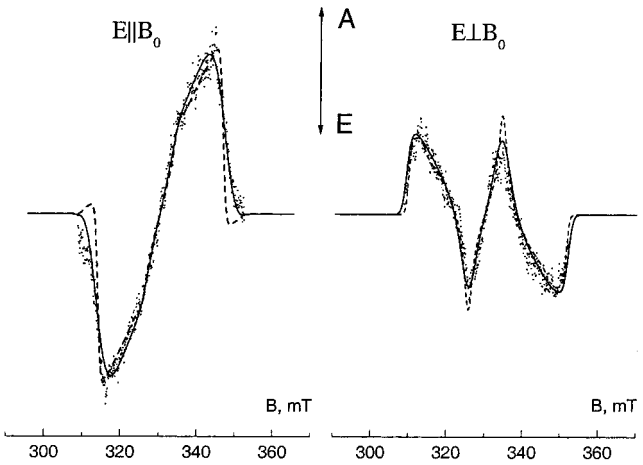


**Figure 2.** Dots: EPR spectra of the $^3$P state detected in the $Q_A$-depleted RCs of *Rb. sphaeroides* R26 under excitation at 850 nm. In contrast to Figure 1, the reaction center preparation was not subjected to additional purification. The other experimental conditions are as in Figure 1. Dashed lines: spectral simulations with $D = 0.0200$ cm$^{-1}$, $E = 0.0040$ cm$^{-1}$, and other parameters as in Figure 1. Solid lines: spectral simulations for normal distributions of the ZFS parameters, $D_0 = 0.0200$ cm$^{-1}$, $\Delta D = 0.0020$ cm$^{-1}$, $E_0 = 0.0040$ cm$^{-1}$, $\Delta E = 0.0030$ cm$^{-1}$. Other parameters as in Figure 1.

"wings" in the $\mathbf{E}||\mathbf{B_0}$ spectrum, which cannot be reproduced by our usual spectral simulation procedure (Figure 2, dashed lines). It can neither be simulated within a two-state model of the primary donor.[36] In addition, excitation of the primary donor in the 880−915 nm range revealed that the ZFS parameters $D$ and $E$ of $^3$P depend on the excitation wavelength (data not shown). This indicates a possibility that the RC preparation used was not completely homogeneous. When we introduced normal distributions of the $D$ and $E$ parameters, the spectra of Figure 2 could be simulated quite well (Figure 2, solid lines). Therefore, it is realistic to assume that the preparation inhomogeneity may affect the shape of the $^3$P spectra and the angular parameters obtained from MPS. In fact, the above-mentioned wings could not be detected in an R26 RC preparation that had been additionally purified on a DEAE-Sephacel column (Figure 1e, f). The MPS spectra of the purified preparation are identical to that of the wild-type RCs. We take this as a proof of conservation of the structure and properties of the primary donor in the RCs of the mutant R26, as compared to *Rb. sphaeroides* 2.4.1. Thus, the data of the single-crystal studies of *Rb. sphaeroides* R26 RCs[33] could be used in our calculations for relating the optical transition moment vectors and magnetic axes systems to the molecular frames.

Figure 3 shows the results of the remaining three MPS experiments (Type 2−Type 4) together with the spectral simulations. A small fraction of the $^3$P signal could be observed overlapping the much larger $^3$Car signal at 100 K (Type 2 and Type 3 experiments). It is most probably due to incomplete transfer of the $^3$P to carotenoid and a small fraction of RCs lacking carotenoid.[37] Because of the sufficiently different $D$ and $E$ values of the $^3$P and $^3$Car EPR signals, it was not difficult to suppress the contamination by subtracting an adequate fraction of the primary donor triplet measured on the R26 reaction centers. Figure 3 shows the high-temperature signals after such subtraction. No indication of spin−lattice relaxation effects reported earlier[27] could be detected in the $^3$Car signals at 100 K. In spectral simulations, the EPR spectroscopic parameters of the $^3$P and $^3$Car signals (ZFS parameters, **g** tensors, line widths) were kept constant, so that only the angular parameters were varied. Their values are collected in Table 1. The errors

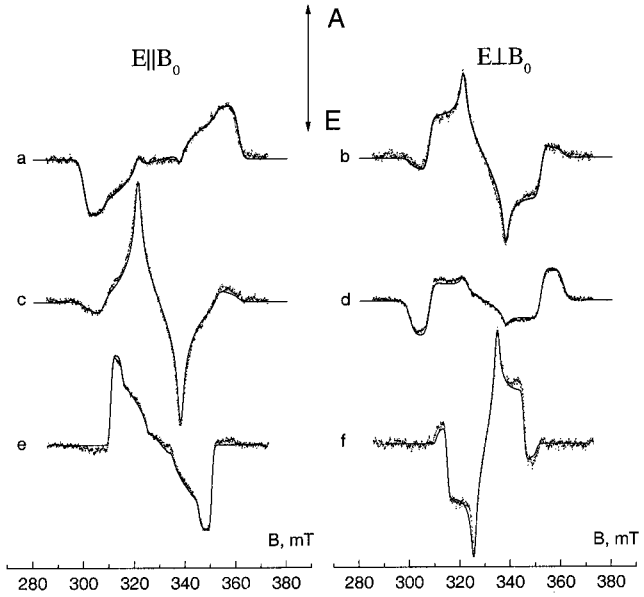


**Figure 3.** EPR spectra obtained in Type 2−Type 4 experiments (dots) and their simulations (solid lines). (a, b): $T = 100$ K, $\lambda_{exc.} = 472$ nm; (c, d): $T = 100$ K, $\lambda_{exc.} = 896$ nm; (e, f): $T = 10$ K, $\lambda_{exc.} = 472$ nm. Simulation parameters for the $^3$P spectrum (curves e, f) are the same as in Figure 1. Simulation parameters for the $^3$Car spectrum (curves a−d) are $D = -0.0285$ cm$^{-1}$, $E = 0.0043$ cm$^{-1}$, $g_x = g_y = 2.002$, $g_z = 2.000$, $\Delta H_x = 2.5$ mT, $\Delta H_y = 1.5$ mT, $\Delta H_z = 2.5$ mT. Values of the best-fit angular parameters $\delta$, $\gamma$ are given in Table 1.

**TABLE 1: Best-Fit Angular Parameters for Wild-Type RCs**

| | $\boldsymbol{Q}_Y$ rel. $^3$P axes | $\boldsymbol{Q}_Y$ rel. $^3$Car axes | $\boldsymbol{D}$ rel. $^3$P axes | $\boldsymbol{D}$ rel. $^3$Car axes |
|---|---|---|---|---|
| $\delta$ | 90° ± 10° | 75° ± 3° | 26° ± 2° | 28° ± 2° |
| $\gamma$ | 90° ± 10° | 75° ± 5° | 58° ± 10° | 50° ± 7° |

given represent maximum deviations, estimated by varying $\delta$, $\gamma$ until the difference between simulated and experimental spectra became apparent by eye.

**Orientation of the Spheroidene Optical Transition Moment.** In the Type 4 experiment, the orientation of the spheroidene optical transition moment $\boldsymbol{D}$ relative to the $^3$P magnetic axes is determined, which enables the calculation of the orientation of $\boldsymbol{D}$ relative to the molecular structure of the carotenoid. To this purpose, the average structural axes of P were first calculated (called earlier the "X-ray axes"[33]), and then, the information on the $^3$P principal axes orientation relative to the structural axes were utilized (Table 4 in ref 33). As the result, the coordinates of $\boldsymbol{D}$ vector in the structural system are obtained, which can be used to overlay this vector on the molecular frame of spheroidene. Since spheroidene does not undergo conformational changes when promoted from the ground state into its triplet state,[38,39] we can utilize the X-ray structure of the RC obtained for the ground state of the carotenoid for studying an excited state. Apart from the orientation of the optical transition moment of spheroidene $\boldsymbol{D}$ given in Table 1, there are three other orientations of $\boldsymbol{D}$ relative to the $^3$P principal axes system which correspond to the measured MPS spectra. To select a unique optical transition moment orientation, additional physical considerations have to be applied. In linear polyenes such as carotenoids in the all-trans state, the optical transition moment lies along the molecule. In the cis state present in RCs,[40−42] an additional cis band appears at shorter wavelength from the main $S_2 \leftarrow S_0$ transition.[43] The 472-nm band used for the excitation in the present work is the strongest vibronic peak of the main transition; it thus should correspond to a shift of the electron density on excitation along the molecular frame. For the approximate $C_{2v}$ symmetry of the 15,15′-cis RC carotenoid, one then expects the 472-nm optical transition moment to be oriented perpendicular to its $C_2$ axis. If we consider the carotenoid molecule bound to RC as a bow, the carotenoid optical transition moment $\boldsymbol{D}$ will be then directed along the bowstring. As the photophysical properties of carotenoids are largely determined by the atoms participating in the double-bond conjugation,[44,45] in the following we will consider only this region of the spheroidene molecule.

The four calculated orientations of the optical transition moment $\boldsymbol{D}$ were compared with the average double-bond direction of spheroidene (that is, the line connecting the ends of the double-bond region, carbon atoms C2−C8′). Two orientations were discarded as they deviated too far from the expected direction (by ≥40°). Later, checks of these orientations for the triplet magnetic axes systems to which they correspond (see below) showed that such operation was justified. The other two orientations are making angles within 13° with the average plane of the double-bond region. They were treated explicitly up to the stage of the $^3$P principal magnetic axes calculation. This enabled the determination of a single optical transition moment orientation (making an angle of 20°) with the "bowstring", which was in accord with the principal triplet system as well.

**Calculation of the Spheroidene Triplet Magnetic Axes System Relative to the Molecular Frame.** The four types of the MPS experiments provide information of how the two vectors, $\boldsymbol{Q}_Y$ and $\boldsymbol{D}$, are oriented relative to the two triplet magnetic axes systems—that of $^3$P, whose orientation relative to the crystallographic coordinates has been determined,[33] and that of the $^3$Car system with unknown triplet axes coordinates. In principle, the values of the coordinates of two noncollinear vectors define an axes system, so it is possible to calculate the orientation of the $^3$Car magnetic axes system relative to the molecular frame as well. Here again one encounters the problem of multiple possible orientations of the optical transition moment vectors allowed by MPS. Thus, all possible orientations have to be considered and the corresponding principal triplet axes calculated and overlaid on the RC X-ray structure, and then their comparison performed, on the basis of general physical principles. The $\boldsymbol{Q}_Y$ orientation in the $^3$P magnetic axes system is close to $\delta = 90°$, $\gamma = 90°$ ($\boldsymbol{Q}_Y$ parallel to the $y$-triplet axis of the primary donor). In this case, there are only two MPS allowed orientations of the vector (parallel or antiparallel to $y$), which are equivalent. Small rotations of $\boldsymbol{Q}_Y$ within the error limits of $\delta$, $\gamma$ alter the situation insignificantly and will be dealt with in the Discussion section. As mentioned above, there are four variants for the $\boldsymbol{D}$ orientation in the $^3$P principal axes system, of which only two will be considered at the moment. We thus limit ourselves to two different orientations of $\boldsymbol{Q}_Y$ and $\boldsymbol{D}$ vectors in the $^3$P magnetic system relative to each other. In the $^3$Car principal axes system, the situation is much more complicated because now none of the vectors are parallel to a triplet axis and there are four variants for each vector, which gives $4 \times 4 = 16$ variants of the relative orientations of the vectors. Each orientation of the two vectors in the $^3$P and $^3$Car magnetic axes systems gives rise to a triplet axes system of spheroidene relative to the crystallographic coordinates, thus the full number of solutions is $16 \times 2 = 32$. The number of variants sufficiently decreases under the condition that the angle between $\boldsymbol{Q}_Y$ and $\boldsymbol{D}$ vectors has to be preserved in any coordinate system, so in the $^3$Car magnetic system within the error limits it should be equal to 68° ± 10°, as is observed in the $^3$P magnetic system. This enables sorting out three-fourths of the vector combinations,

leaving only eight of them. The search for the $^3$Car magnetic axes systems corresponding to the remaining combinations was performed in the following way. The $^3$P magnetic axes system, whose orientation relative to the crystallographic coordinates is known, was rotated consecutively around its *x*, *y*, *z* axes in the 0−360° range in steps of 1°. The $\delta$, $\gamma$ angles of the $\boldsymbol{Q_Y}$ and $\boldsymbol{D}$ vectors determined in the $^3$P magnetic system were calculated relative to the rotated system and compared to the values obtained experimentally for the optical transition moments in the $^3$Car magnetic axes system. When the corresponding angles coincided within the error limits presented in Table 1, this was considered as a solution for the particular $^3$Car magnetic axes system. The procedure resulted in a region of possible orientations for the spheroidene triplet axes, the center of which was taken as the orientation of the $^3$Car magnetic system relative to the $^3$P magnetic axes system. Eight sets of the triplet axes were obtained in this way and could be recalculated to the crystallographic coordinates in the same way as for the $\boldsymbol{D}$ optical transition moment. They split into four pairs of equivalent coordinate system, differing by a 180° rotation around the *x*-axis. We are thus left with four possible orientations of the $^3$Car magnetic axes systems. To choose between them, one has to rely upon their general properties.

From earlier studies of the $^3$Car state in *Rb. sphaeroides* 2.4.1., it is known that its magnetic axes are not equivalent. The analysis of the DDEPR-measured signals of the spheroidene triplet demonstrated[46] that the second EPR transition (counted from low to high field) decayed to the ground state considerably slower than the other two transitions. The axis 2 is therefore expected to have an appreciably lower projection on the spheroidene molecule than the other two axes.[46−48] For spheroidene in RC, $D < 0$ but the sign of $E$ is unknown. If $E > 0$, the order of the canonical transitions in the EPR triplet state spectrum of Car will be Z−X−Y−Y−X−Z, and the axis labeled earlier as 2 will be actually the *x*-axis of the $^3$Car. On the other side, if $E < 0$, the inverse order of the central canonical peaks will be expected and axis 2 will be the *y*-axis of the $^3$Car. Since we cannot distinguish between these two cases, we will assume that $E > 0$. If $E < 0$, then the *x* and *y* labels should be exchanged. The four pairs of the triplet coordinate systems were thus compared with respect to their *x*-axis orientation relative to the molecule of spheroidene. An average plane for the carotenoid carbon atoms participating in the double-bond conjugation was constructed, and projections of the *x*-axis on the plane were calculated. A single pair of equivalent triplet axes was found, with the *x*-axis close to perpendicular (84°) to that plane. The other three pairs of coordinate systems do not possess an *x* magnetic axis that would be oriented relative to the spheroidene molecule in a way sufficiently different from the other two axes and thus do not account for the relaxation properties of $^3$Car state.[46] Coming back to the orientation of $\boldsymbol{D}$, this triplet axis system defines a single orientation of the optical transition moment, viz., the one with the 20° deviation from the average double-bond direction. Analogous calculations performed with the two $\boldsymbol{D}$ orientations discarded earlier because of their large deviation from the average double-bond direction resulted in none of these triplet axes systems having an *x*-axis orientation sufficiently different from the *y*- and *z*-axes orientations.

In Figure 4, the calculated optical transition moments and principal triplet axes of P and Car are overlaid on the X-ray structure of the *Rb. sphaeroides* 2.4.1. reaction center (1PSS entry of the Protein Data Bank[34]). The 2-fold symmetry axis $C_2$, constructed by connecting the center of the Mg−Mg line

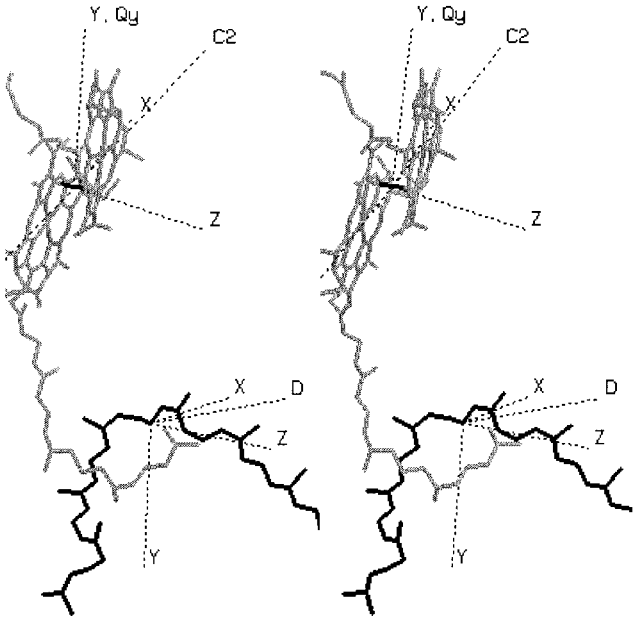


**Figure 4.** Stereopair of the part of the 1PSS structure with the primary donor (shown in gray) and spheroidene (shown in black) molecular axes overlaid.

**TABLE 2: Projections of $^3$Car Axes and of *D* Vector onto the PDB Coordinate System of the 1PSS Structure Used To Construct Figure 4**

| | PDB *x*-axis | PDB *y*-axis | PDB *z*-axis |
|---|---|---|---|
| $^3$Car *x*-axis | 0.3807 | 0.7325 | −0.5644 |
| $^3$Car *y*-axis | −0.8745 | 0.0989 | −0.4747 |
| $^3$Car *z*-axis | −0.2702 | 0.6856 | 0.6760 |
| *D* | −0.4314 | 0.8662 | 0.2516 |

of the primary donor BChls and the non-heme $Fe^{2+}$ ion, is also shown. The $C_2$ direction is thought to be perpendicular to the photosynthetic membrane incorporating the RC in vivo.[49] For clarity of presentation, only the BChls of the primary donor P and the spheroidene molecule are shown. In P, the optical transition moment $\boldsymbol{Q_Y}$ coincides with the *y*-triplet axis of primary donor and makes an angle of 89° with the $C_2$ axis. For Car, the optical transition moment $\boldsymbol{D}$ makes an angle of 73° with the $C_2$ axis. It is tilted out of the average spheroidene plane by 8°. The orientations of the $^3$Car principal magnetic axes and of the optical transition moment $\boldsymbol{D}$ relative to the crystallographic axes of the 1PSS structure, used for drawing Figure 4, are summarized in Table 2. In the 1PSS structure (obtained with 3 Å resolution), the position of spheroidene is well defined, but its configuration for the location of the cis bond is less reliable.[34] This could affect the precision of the overlay procedure reported in the present work. Recently, a better-resolved 1QOV structure (2.1 Å resolution) of the AM260W *Rb. sphaeroides* mutant has been published.[50] In this structure, both the position and configuration of carotenoid are well defined. The mutated Ala M260 is located near the $Q_A$ site of the RC, and its exchange for Trp is not expected to cause sizable changes in the primary donor carotenoid region. Though this reaction center contains spheroidenone instead of spheroidene, we overlaid the calculated optical and triplet axes on the carotenoid of 1QOV. The axes orientations relative to the molecular frame appeared to be within 2° of that in the 1PSS structure. This is not surprising as the conjugated double-bond parts of the two carotenoids overlap nicely; for example, the bowstrings of the molecules are only 1.4° apart.

**MPS of *Rb. sphaeroides* R26 Reaction Centers Reconstituted with Spheroidene.** Reaction centers of the carotenoidless

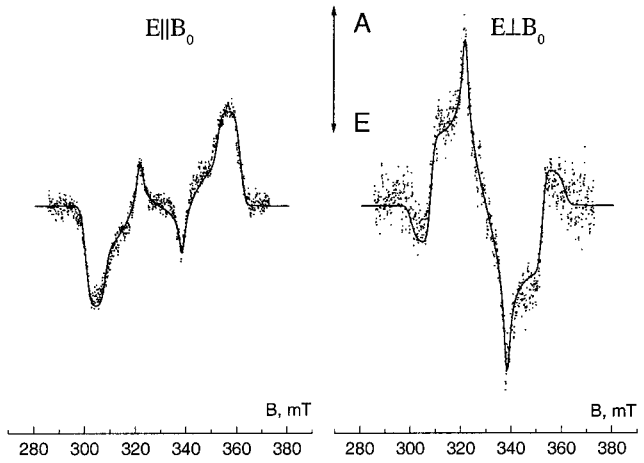


**Figure 5.** EPR spectra obtained in the Type 3 experiment ($T = 100$ K, $\lambda_{exc.} = 472$ nm) with *Rb. sphaeroides* R26 RCs reconstituted with spheroidene (dots) and their simulations (solid lines). Spectroscopic parameters of the simulation are the same as for the $^3$Car spectrum in Figure 3. Values of the best-fit angular parameters $\delta$, $\gamma$ for this and other three types of experiments are given in Table 3.

**TABLE 3: Best-Fit Angular Parameters for R26 RCs Reconstituted with Spheroidene**

| | $\boldsymbol{Q_Y}$ rel. $^3$P axes | $\boldsymbol{Q_Y}$ rel. $^3$Car axes | $\boldsymbol{D}$ rel. $^3$P axes | $\boldsymbol{D}$ rel. $^3$Car axes |
|---|---|---|---|---|
| $\delta$ | $90° \pm 10°$ | $73° \pm 3°$ | $27° \pm 2°$ | $38° \pm 2°$ |
| $\gamma$ | $90° \pm 10°$ | $67° \pm 5°$ | $60° \pm 10°$ | $50° \pm 7°$ |

mutant *Rb. sphaeroides* R26 are readily reconstituted with different carotenoids when incubated in solution in their presence.[30,51,52] For RC preparation reconstituted with spheroidene, we have performed the same four types of MPS experiments as described above. The angles providing best fits of the experimental spectra are given in Table 3. As can be seen, the values are slightly different from that of wild-type RCs, especially the spherical angle $\delta$ for the orientation of the $\boldsymbol{D}$ relative to $^3$Car magnetic axes system. This difference is apparent already in the MPS spectra, as can be seen in Figure 5 (compare with Figure 3a, b). We take this as an indication for a slightly different orientation and conformation of the spheroidene molecule as compared to nontreated reaction centers of *Rb. sphaeroides* 2.4.1.

## Discussion

**Principal Triplet Axes of Spheroidene. Error Estimation.** The coordinates of the $^3$P magnetic axes system in the crystallographic axes have been determined earlier,[33] and the uncertainty has been estimated as ca. $\pm 1°$. The orientation of the spheroidene triplet axes relative to the molecular structure has been determined here for the first time. It is thus especially important to estimate the precision of this determination. The procedure of finding the $^3$Car principal axes was numerical, precluding us to perform an analytical error calculation. Therefore, we adopted an alternative approach. The triplet axes were calculated for each orientation of $\boldsymbol{Q_Y}$ and $\boldsymbol{D}$ vectors relative to the $^3$P and $^3$Car magnetic axes that lie within the error limits of these vectors, with a step of 1° and 3°, respectively. This operation produced ca. 3000 solutions for the $^3$Car axes orientation. The projections of these axes on the $^3$P axes system were distributed around their average values in a bell-shape manner. In the next step, the statistical formalism for Gaussian distributions was applied, and standard deviation values were obtained. This approach is not mathematically strict. However, it seems to us realistic enough for the following reason. The wings of the distribution correspond to the case when the errors estimated from MPS spectra are close to their maximum values. We assume that the situation when all or the majority of the angular parameters simultaneously reach their outermost values has low probability. This draws the calculated distribution of the axes system nearer to a statistical case. The uncertainty fields for the $^3$Car principal axes system relative to the molecular structure are then described as cones with an angle of $\pm 9°$.

A possible source of systematic error is the nonselectivity of carotenoid excitation at 472 nm. In addition to spheroidene, the bacteriochlorophylls and bacteriopheophytins of the RC absorb at that wavelength, though much weaker than the carotenoid. Absorption spectra of the R26 and 2.4.1. RC preparations measured under conditions similar with EPR (helium-range temperature with 66% (v/v) of glycerol) revealed that about 85% of the absorbed quanta excite spheroidene. This excitation energy is transferred to P with about 80% efficiency at room temperature, which does not substantially change when temperature is lowered from 77 to 5 K.[16] In the least favorable case when there is only one other absorbing type of molecule with its optical transition moment orthogonal to that of spheroidene, this other absorption will introduce an error of less than 10°. Control measurements of MPS on *Rb. sphaeroides* R26 mutant RCs with 472 nm excitation of only chlorophyll-type pigments revealed a very low degree of photoselection (data not shown). In accord, zero photoselection has been observed earlier[53] in photodichroism study with excitation into the carotenoid region of *Rb. sphaeroides* R26. It means that there are several pigments absorbing at 472 nm, with differently oriented optical transition moments, so that partial averaging of MPS takes place. This effect diminishes the error due to nonselective absorption. As the data on MPS in *Rb. sphaeroides* 2.4.1. RCs (Figure 3) show no admixture of nonphotoselected spectra, the effect of nonselective absorption on calculated angles was assumed to be negligible.

**Comparison with Previous Data.** The orientation of the spheroidene optical transition moment and its triplet axes has been extensively studied before, both with optical and EPR spectroscopy. Photodichroism studies of *Rb. sphaeroides* 2.4.1. RCs enabled determination of an angle of ca. 70° between $\boldsymbol{Q_Y}$ and $\boldsymbol{D}$ vectors,[53] which is in very good agreement with the value of $68° \pm 10°$ calculated from our MPS measurements. The value of 67° was obtained also from optical linear dichroism measurements on single crystals of *Rb. sphaeroides* 2.4.1 RCs.[54] The finding that $\boldsymbol{Q_Y}$ is parallel to the photosynthetic membrane[49,55] agrees nicely with the angle of 89° between $\boldsymbol{Q_Y}$ vector and the $C_2$ axis derived from our MPS measurements.

Investigations of the $^3$Car magnetic axes have been carried out for several years by H. Frank et al.[25,26,46,55] Table 4 compares the orientations of the $\boldsymbol{Q_Y}$ and $\boldsymbol{D}$ vectors relative to the $^3$Car magnetic axes obtained from MPS measurements by that group[26] and in the present work. In Table 5, such comparison is made for the angles of the $^3$Car axes relative to the $C_2$ axis of the RC. From Table 4, it is apparent that except for the orientation of $\boldsymbol{D}$ in the $^3$Car axes system, the data of the present work differ considerably from previous results. Also, the angles for the orientation of $^3$Car axes relative to the $C_2$ axis obtained in this work and those in ref 55 (Table 5) differ considerably. We believe that these differences are largely due to the inadequacy of the steady-state MPS technique with CW EPR used earlier for the studies of dynamic paramagnetic states. Let us consider this problem in more detail. The CW EPR spectra are essentially steady-state ones, thus they represent the time average of

**TABLE 4: Projections of the $Q_Y$ and $D$ Optical Transition Moments onto the $^3$Car Magnetic Axes**

| | $Q_Y$ | | | $D$ | | |
|---|---|---|---|---|---|---|
| | *x* | *y* | *z* | *x* | *y* | *z* |
| ref 26 | 0.72 ± 0.08 | 0.60 ± 0.07 | 0.32 ± 0.08 | 0.37 ± 0.03 | 0.42 ± 0.02 | 0.82 ± 0.03 |
| this work[a] | 0.25 ± 0.09 | 0.93 ± 0.04 | 0.25 ± 0.05 | 0.30 ± 0.06 | 0.36 ± 0.06 | 0.88 ± 0.02 |

[a] Absolute values given.

**TABLE 5: Orientation of the $^3$Car Triplet Axes Relative to the $C_2$ Axis of the Reaction Center**

| axes | this work[a] | ref 55 |
|---|---|---|
| *x* | 20 | 40 |
| *y* | 70 | 53 |
| *z* | 85 | 78 |

[a] Errors ±9°.

photoinduced signals. As in the approach adopted in the present work and in ref 27, spectral simulation in previous studies[56] was started with the calculation of the "isotropic" spectrum, that is, the spectrum arising when all orientations of the absorbing molecules in a sample are excited with equal probability. Spin−lattice relaxation of $^3$Car was neglected because it was assumed to be slower than the triplet depopulation to the ground state, and the deviations of the canonical lines amplitudes from theoretical values were accounted for by introducing depopulation rate constants of the spin sublevels. The kinetic parameters obtained from simulation of the isotropic spectrum were subsequently introduced into the MPS calculations, resulting in the angular parameters. However, the spectrum excited under standard EPR conditions cannot be considered as isotropic.[27] The assumption of its isotropic character brings errors into the estimated kinetic parameters and finally into the values of the angular coordinates of the optical transition moments. In our calculations, the $\mathbf{E}||\mathbf{B_0}$ and $\mathbf{E}\perp\mathbf{B_0}$ spectra were measured separately, and the isotropic spectrum was constructed as a sum of one $\mathbf{E}||\mathbf{B_0}$ spectrum with two $\mathbf{E}\perp\mathbf{B_0}$ spectra. In addition, demands for the simulation precision in the DDEPR-detected spectra are higher than for the CW ones, which are in the derivative presentation. The "integrated" DDEPR spectra have to be carefully calculated throughout the whole spectral range, in contrast to CW EPR spectra which show large amplitudes mostly around the canonical fields, where the derivative of the spectral line becomes large. Moreover, the DDEPR spectra are essentially free from spin−lattice relaxation effects. All this results in an improved reliability of the angular coordinates obtained from DDEPR MPS.

**Conformation of Spheroidene in Carotenoid-Reconstituted RCs.** It is generally accepted that spheroidene (all-trans isomer in solution) reconstituted into the carotenoidless *Rb. sphaeroides* mutant R26 acquires a 15,15′-cis configuration very similar or identical to that of carotenoid in wild-type reaction centers. Our data indicate that this similarity is not perfect (cf. Table 1 and Table 3). Although the orientation of the optical transition moment $\boldsymbol{D}$ relative to the RC structure coincides in the two preparations perfectly, its orientation in the $^3$Car axes system is rotated a few degrees outside the error margin. We interpret this variation as being due to a slightly different conformation of the spheroidene molecules in the native and reconstituted preparations, which alters the triplet axes system keeping the direction of the optical transition moment constant. Certain differences in the spheroidene resonance Raman spectra have been reported earlier for the same kind of preparations[51] and have been interpreted as slight differences between the conformations of native and reconstituted spheroidene. One of the possible explanations for the difference between native and reconstituted spheroidene is a twist at the 6−7 or 6′−7′ positions of the spheroidene that may occur upon its binding to the reaction center protein.[57]

## Conclusions

This work shows that magnetophotoselection with direct-detection EPR enables one to obtain precise orientations of the optical transition moments relative to the triplet magnetic axes system even in the case of short-lived states with fast spin−lattice relaxation rate. The relative orientations of the optical transition moments and the triplet magnetic axes of the primary donor and carotenoid molecules in bacterial reaction centers of *Rb. sphaeroides* 2.4.1. were determined. For the first time, using the above techniques and earlier data on the $^3$P principal magnetic axes orientation in the molecular frame, we were able to determine the orientation of the optical transition moment and the triplet axes system of spheroidene in the molecular frame of spheroidene in the reaction center. Our data indicate that spheroidene reconstituted into the carotenoidless mutant *Rb. sphaeroides* R26 has a slightly different orientation or conformation compared to the native carotenoid in wild-type reaction centers.

**Acknowledgment.** We are thankful to Mr. Bram Joosten for the RC preparations. This work was supported by The Netherlands Foundation for Chemical Research (SON), financed by The Netherlands Organization for Scientific Research (NWO). I.B.K. thanks INTAS and NWO for travel support (grants No. 93-2849-ext and 47-006-003). I.I.P. acknowledges financial support of FOM (Dutch Foundation for Fundamental Studies of Matter) and of the Russian Science Foundation RFBR (grant 99-04-48184).

## References and Notes

(1) Siefermann-Harms, D. *Biochim. Biophys. Acta* **1985**, *811*, 325.
(2) Cogdell, R. J.; Frank, H. A. *Biochim. Biophys. Acta* **1987**, *895*, 63.
(3) Frank, H. A. In *The Photosynthetic Reaction Center*; Deisenhofer, J., Norris, J. R., Eds.; Academic Press: New York, 1993; Vol. 2, p 221.
(4) Boucher, F.; van der Rest, M. *Biochim. Biophys. Acta* **1977**, *461*, 339.
(5) Frank, H. A.; Bautista, J. A.; Josue, J.; Pendon, Z.; Hiller, R. G.; Sharples, F. P.; Gosztola, D.; Wasielewski, M. R. *J. Phys. Chem.* **2000**, *104B*, 4569.
(6) Frank, H. A.; Bolt, J. D.; de Costa, S. M. B.; Sauer, K. *J. Am. Chem. Soc.* **1980**, *102*, 4893.
(7) Nuijs, A. M.; van Grondelle, R.; Joppe, H. L. P.; van Bochove, A. C.; Duysens, L. N. M. *Biochim. Biophys. Acta* **1985**, *810*, 94.
(8) Frick, J.; von Schutz, J. U.; Wolf, H. C.; Kothe, G. *Mol. Cryst. Liq. Cryst.* **1990**, *183*, 269.
(9) Rademaker, H.; Hoff, A. J.; van Grondelle, R.; Duysens, L. N. M. *Biochim. Biophys. Acta* **1980**, *592*, 240.
(10) Chauvet, J.-P.; Bazin, M.; Santus, R. *Photochem. Photobiol.* **1985**, *41*, 83.
(11) Parson, W. W.; Cogdell, R. J. *Biochim. Biophys. Acta* **1975**, *416*, 105.
(12) Thurnauer, M. C.; Katz, J. J.; Norris, J. R. *Proc. Natl. Acad. Sci. U.S.A.* **1975**, *72*, 3270−3274.
(13) Hoff, A. J.; Proskuryakov, I. I. *Chem. Phys. Lett.* **1985**, *115*, 303.
(14) Wraight, C. A.; Leigh, J. S.; Dutton, P. L.; Clayton, R. H. *Biochim. Biophys. Acta* **1974**, *333*, 401.
(15) Schenck, C. C.; Blankenship, R. E.; Parson, W. W. *Biochim. Biophys. Acta* **1982**, *680*, 44.

(16) Schenck, C. C.; Mathis, P.; Lutz, M. *Photochem. Photobiol.* **1984**, *39*, 407.

(17) Frank, H. A.; Violette, C. A. *Biochim. Biophys. Acta* **1989**, *967*, 222.

(18) De Winter, A.; Boxer, S. G. *J. Phys. Chem.* **1999**, *103B*, 8786.

(19) Budil, D. E.; Thurnauer, M. C. *Biochim. Biophys. Acta* **1991**, *1057*, 1.

(20) Angerhofer, A. In *Chlorophylls*; Scheer, H., Ed.; CRC Press: Boca Raton, FL, 1991; p 945.

(21) Hoff, A. J.; Deisenhofer, J. *Phys. Rep.* **1997**, *287*, 1.

(22) Cogdell, R. J.; Monger, T. G.; Parson, W. W. *Biochim. Biophys. Acta* **1975**, *408*, 189.

(23) Monger, T. G.; Cogdell, R. J.; Parson, W. W. *Biochim. Biophys. Acta* **1976**, *449*, 136.

(24) Frank, H. A.; Machnicki, J.; Felber, M. *Photochem. Photobiol.* **1982**, *35*, 713.

(25) Frank, H. A.; Machnicki, J.; Friesner, R. *Photochem. Photobiol.* **1983**, *38*, 451.

(26) McGann, W. J.; Frank, H. A. *Biochim. Biophys. Acta* **1985**, *807*, 101.

(27) Borovykh, I. V.; Proskuryakov, I. I.; Klenina, I. B.; Gast, P.; Hoff, A. J. *J. Phys. Chem.* **2000**, *104B*, 4222.

(28) Feher, G.; Okamura, M. In *The Photosynthetic Bacteria*; Clayton, R. K., Sistrom, W. R., Eds.; Plenum Press: New York, 1978; Chapter 19.

(29) Cogdell, R. J.; Durrant, I.; Valentine, J.; Lindsay, J. G.; Schmidt, K. *Biochim. Biophys. Acta* **1983**, *722*, 427.

(30) Chadwick, B. W.; Frank, H. A. *Biochim. Biophys. Acta* **1986**, *851*, 257.

(31) Bosch, M. K.; Proskuryakov, I. I.; Gast, P.; Hoff, A. J. *J. Phys. Chem.* **1996**, *100*, 2384.

(32) Otte, S. M. C. Doctoral Thesis, Leiden University, Leiden, The Netherlands, 1992.

(33) Norris, J. R.; Budil, D. E.; Gast, P.; Chang, C.-H.; El-Kabbani, O.; Schiffer, M. *Proc. Natl. Acad. Sci. U.S.A.* **1989**, *86*, 4335.

(34) Yeates, T. O.; Komiya, H.; Chirino, A.; Rees, D. C.; Allen, J. P.; Feher, G. *Proc. Natl. Acad. Sci. U.S.A.* **1988**, *85*, 7993.

(35) Allen, J. P.; Feher, G.; Yeates, T. O.; Komiya, H.; Rees, D. C. *Proc. Natl. Acad. Sci. U.S.A.* **1987**, *84*, 5730.

(36) Müh, F.; Rautter, J.; Lubitz, W. *Biochemistry* **1997**, *36*, 4155.

(37) *The Photochemistry of Carotenoids*; Frank, H. A., Young, A. J., Britton, G., Cogdell, R. J., Eds.; Advances in Photosynthesis, Vol. 8; Kluwer: Dordrecht, The Netherlands, 1999.

(38) Lutz, M.; Chinski, L.; Turpin, P. Y. *Photochem. Photobiol.* **1982**, *36*, 503.

(39) Robert, B.; Szponarski, W.; Lutz, M. In *Time-resolved Vibrational Spectroscopy*; Laubereau, A., Stockburger, M., Eds.; Springer: Berlin, 1985; p 220.

(40) Lutz, M.; Agalidis, I.; Hervo, G.; Cogdell, R. J. *Biochim. Biophys. Acta* **1978**, *503*, 287.

(41) Koyama, Y.; Kito, M.; Takii, T.; Saiki, K.; Tsukida, K.; Yamashita, J. *Biochim. Biophys. Acta* **1982**, *680*, 109.

(42) Robert, B. *Biochim. Biophys. Acta* **1990**, *1017*, 99.

(43) Zechmeister, L. *Cis−trans Isomeric Carotenoids, Vitamins A and Arylpolyenes*; Academic Press: New York, 1962.

(44) Angerhofer, A.; Börnhauser, F.; Gall, A.; Cogdell, R. *Chem. Phys.* **1995**, *194*, 259.

(45) Kohler, B. E. In *Carotenoids*, Vol. 1B: Spectroscopy; Britton, G., Liaaen-Jensen, S., Pfander, H., Eds.; Birkhauser Verlag: Basel, 1995; p 3.

(46) McGann, W. J.; Frank, H. A. *Chem. Phys. Lett.* **1985**, *121*, 253.

(47) Metz, F.; Friedrich, F.; Hohlneicher, G. *Chem. Phys. Lett.* **1972**, *16*, 353.

(48) Henry, B. R.; Siebrand, W. *J. Chem. Phys.* **1972**, *54*, 1072.

(49) Breton, J. *Biochim. Biophys. Acta* **1985**, *810*, 235.

(50) McAuley, K. E.; Fyfe, P. K.; Ridge, J. P.; Isaacs, N. W.; Cogdell, R. J.; Jones, M. R. *Proc. Natl. Acad. Sci. U.S.A.* **1999**, *96*, 14706.

(51) Agalidis, I.; Lutz, M.; Reiss-Husson, F. *Biochim. Biophys. Acta* **1980**, *589*, 264.

(52) Frank, H. A.; Chadwick, B. W.; Taremi, S.; Kolaczkowski, S.; Bowman, M. *FEBS Lett.* **1986**, *203*, 157.

(53) Vermeglio, A.; Breton, J.; Paillotin, G.; Cogdell, R. *Biochim. Biophys. Acta* **1978**, *501*, 514.

(54) Frank, H. A.; Violette, C. A.; Taremi, S. S.; Budil, D. E. *Photosynth. Res.* **1989**, *31*, 107.

(55) Frank, H. A.; Machnicki, J.; Toppo, P. *Photochem. Photobiol.* **1984**, *39*, 429.

(56) Frank, H. A.; Friesner, R.; Nairn, J. A.; Dismukes, G. C.; Sauer, K. *Biochim. Biophys. Acta* **1979**, *547*, 484.

(57) Frank, H. A.; Cogdell, R. J. In *Carotenoids in Photosynthesis*; Young, A., Britton, G., Eds.; Chapman & Hall: London, 1993; p 253.